Greenland Ice Sheet Surface Air Temperature Variability: 1840–2007*

JASON E. BOX

Byrd Polar Research Center, and Department of Geography, Atmospheric Sciences Program, The Ohio State University, Columbus, Ohio

LEI YANG

Key Laboratory of Tropical Marine Environmental Dynamics, South China Sea Institute of Oceanology, Chinese Academy of Sciences, Guangzhou, China

DAVID H. BROMWICH

Byrd Polar Research Center, and Department of Geography, Atmospheric Sciences Program, The Ohio State University, Columbus, Ohio

LE-SHENG BAI

Byrd Polar Research Center, The Ohio State University, Columbus, Ohio

(Manuscript received 2 September 2008, in final form 26 January 2009)

ABSTRACT

Meteorological station records and regional climate model output are combined to develop a continuous 168-yr (1840–2007) spatial reconstruction of monthly, seasonal, and annual mean Greenland ice sheet near-surface air temperatures. Independent observations are used to assess and compensate for systematic errors in the model output. Uncertainty is quantified using residual nonsystematic error. Spatial and temporal temperature variability is investigated on seasonal and annual time scales. It is found that volcanic cooling episodes are concentrated in winter and along the western ice sheet slope. Interdecadal warming trends coincide with an absence of major volcanic eruptions. Year 2003 was the only year of 1840–2007 with a warm anomaly that exceeds three standard deviations from the 1951–80 base period. The annual whole ice sheet 1919–32 warming trend is 33% greater in magnitude than the 1994–2007 warming. The recent warming was, however, stronger along western Greenland in autumn and southern Greenland in winter. Spring trends marked the 1920s warming onset, while autumn leads the 1994–2007 warming. In contrast to the 1920s warming, the 1994–2007 warming has not surpassed the Northern Hemisphere anomaly. An additional 1.0°–1.5°C of annual mean warming would be needed for Greenland to be in phase with the Northern Hemispheric pattern. Thus, it is expected that the ice sheet melt rates and mass deficit will continue to grow in the early twenty-first century as Greenland's climate catches up with the Northern Hemisphere warming trend and the Arctic climate warms according to global climate model predictions.

1. Introduction

Climate influences the Greenland ice sheet mass budget, which in turn exerts a significant influence on global sea level (Lemke et al. 2007; Bindoff et al. 2007) and thermohaline circulation (e.g., Fichefet et al. 2003; Rahmstorf et al. 2005). Further, Greenland ice sheet flow dynamics reflect a spectrum of major past climate changes, including the Pleistocene ice age, the Holocene warming that incorporates the Holocene thermal maximum (Kaufman et al. 2004), and warming since 1750 that is caused by a combination of externally and internally forced warming after the Little Ice Age (Crowley 2000; Solomon et al. 2007). Greenland inland ice flow is also sensitive to high-frequency temporal variability, including subseasonal surface melting (Zwally et al. 2002; van de Wal et al. 2008). Satellite and aircraft remote sensing has documented major variability and changes to

* Byrd Polar Research Center Contribution Number 1377.

Corresponding author address: Jason Box, Room 108, Scott Hall, 1090 Carmack Rd., Columbus, OH 43210.
E-mail: box.11@osu.edu

DOI: 10.1175/2009JCLI2816.1

Greenland outlet glaciers and ice sheet mass balance (Joughin et al. 2004; Rignot and Kanagaratnam, 2006; Luthcke et al. 2006; Howat et al. 2008; Joughin et al. 2008; Moon and Joughin, 2008). While recent glacier behavior seems to coincide with surface melting (Rignot et al. 2008), ocean temperatures also play an important role (Holland et al. 2008). Deglaciated land adjacent to outlet glaciers exhibits evidence of glacier advance during the Little Ice Age and the 1960–80 cool periods (Csatho et al. 2008), implying that the ice sheet advanced with climate cooling.

Several studies have analyzed long-term instrumental surface air temperature records from Greenland. Putnins (1970) made a comprehensive study of 1881–1955 temperature data. Box (2002) further examined temporal and spatial patterns using an expanded set (1873–2001) of surface air temperature data. In addition to interdecadal warming and cooling trends and volcanic episodes, the North Atlantic Oscillation (NAO), and perhaps sunspot activity, were among the strongest signals. A review of the Greenland-specific results of Przybylak (1997) and Jones et al. (1999) can be found in Box (2002). Hanna and Cappelen (2003) evaluated Greenland coastal temperature records in context of the NAO for the 1958–2001 period characterized by net cooling. Box and Cohen (2006) expanded on work by Kahl et al. (1993), reporting on seasonal and annual trends in upper-air temperatures of 1964–2005 from twice-daily weather balloon soundings, finding significant covariability between surface air temperature records and the upper-air series. Lower-tropospheric warming from the early 1980s to 2005 dominated the longer 1964–2005 period, which is characterized by cooling from the 1960s to the 1980s. By analyzing the two longest surface air temperature records from the meteorological stations at Nuuk and Ammassalik (i.e., Tasiilaq), Greenland, Chylek et al. (2006) determined that the 1920–30 warming was of a greater magnitude than the 1995–2005 warming. Hanna et al. (2005) evaluated temperature trends and volcanism for the Greenland ice sheet using 40-yr European Centre for Medium-Range Weather Forecasts (ECMWF) Re-Analysis (ERA-40) and ECMWF operational analysis data. Box et al. (2006) examined the spatial patterns of temperature variability for data of limited temporal duration (1988–2004) that reflected surface mass budget component responses to increasing surface air temperatures. Hanna et al. (2008) attributed Greenland warming since the early to mid-1990s to wider hemispheric and global warming.

Using a set of 12 coastal and 40 inland ice surface air temperature records in combination with climate model output, for the first time we reconstruct long-term (1840–2007) monthly, seasonal, and annual spatial patterns of temperature variability over a continuous grid covering Greenland and the inland ice sheet. After calibration and validation of the reconstruction, we analyze seasonal and regional temperature variability and trends. The effect of large volcanic eruptions is further studied. We then further compare the 1919–32 and 1994–2007 warming episodes. We finally make a comparison of Greenland ice sheet surface air temperature temporal variability with that of the Northern Hemisphere (NH) average and infer likely temperature changes of the coming decade.

2. Data

a. Land station air temperature records

The long-term monthly average instrumental near-surface air temperature data used in this study are aggregated from three sources, namely, Vinther et al. (2006, hereafter VIN), Cappelen et al. (2006, hereafter CAP), and data from Pituffik Airport/Thule Air Force Base that were downloaded from the National Aeronautics and Space Administration (NASA) Goddard Institute for Space Studies (GISS) Surface Temperature Analysis (GISTEMP) Web site (online at http://data.giss.nasa.gov/gistemp/; see also Peterson and Vose 1997; Hansen et al. 1999, 2001; Table 1 and Fig. 1). VIN contains the longest available records from three sites situated along the south and west coasts. VIN data have been corrected for temporal homogeneity problems and some gaps are filled using statistical regression with nearby stations. CAP include long-term data from Upernavik, that have gaps totaling 4 yr filled using multiple regressions with the Ilulissat and Pituffik records. Northern Hemisphere temperature anomalies that include ocean surface air temperature observations were obtained from GISS and are an 11 January 2008 update of Hansen et al.'s (1999) Fig. 5. The GISTEMP Web site contains further details.

b. Inland ice air temperature records

Inland ice near-surface air temperature data were obtained from Ohmura (1987) and the Greenland Climate Network (GC-Net; see Steffen et al. 1996; Steffen and Box 2001). Additional ice station data from near the ice sheet topographic summit, with gaps filled by daily passive microwave retrieval, are from Shuman et al. (2001). The longest inland ice in situ surface air temperature record used in this study is 9 yr; see Table 2. The longest inland ice surface air temperature records begin in mid-1990 (Ohmura et al. 1991; Steffen et al. 1996) and mid-1991 (Oerlemans and Vugts 1993).

TABLE 1. Coastal near-surface air temperature data used in this study, sorted by duration.

Site name/former name	World Meteorological Organization (WMO) station No.	Latitude (°N)	Longitude (°W)	Time span*	Time span (yr)	Missing data* (%)	Source
Nuuk/Godthåb	4250	64.2	51.8	1785–2005	223	27.8	VIN; CAP
Qaqortoq/Julianehaab	4272	60.7	46.1	1809–2007	199	32.7	VIN; CAP
Ilulissat/Jakobshavn	04221 and 04216	69.2	51.1	1813–2007	195	15.4	VIN; CAP
Upernavik	4210	72.8	56.2	1873–2007	135	0.0	CAP
Tasiilaq/Angmagssalik	4360	65.6	37.6	1895–2007	113	0.9	CAP
Ivittuut/Ivigtut	34262	61.2	48.2	1873–1965	93	0.0	CAP
Illoqqortoormiut	4339	70.4	22.0	1948–2007	60	36.7	CAP
Danmarkshavn	4320	76.8	18.8	1949–2007	59	6.8	CAP
Aasiaat/Egedesminde	4220	68.7	52.8	1950–2007	58	0.0	CAP
Prins Christian Sund	4390	60.0	43.2	1950–2007	58	3.4	CAP
Pituffik/Thule Air Force Base	4202	76.5	68.8	1961–2007	47	4.3	GISS; CAP
Narsarssuaq	4270	61.2	45.4	1961–2007	47	4.3	CAP

* Annual averages are used, where available.

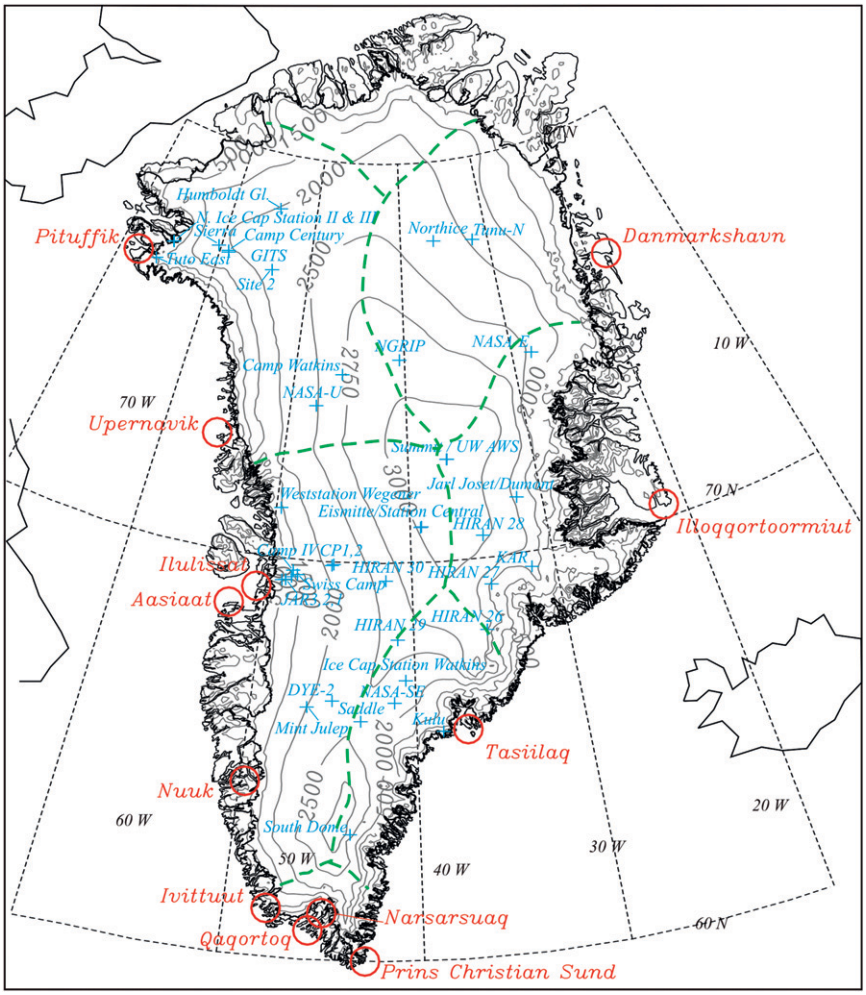

FIG. 1. Location map of surface air temperature records used in this study. Boundaries of ice sheet drainage basins referred to as climate regions are indicated (green dashed lines). Elevation contours (in m ASL) are gray.

TABLE 2. Inland ice station near-surface air temperature data used in this study; sites are sorted by number of monthly averages.

Ice station name	Station No.	Latitude (°N)	Longitude (°W)	Elevation (m)	Time span	No. of months	Data source
University of Wisconsin (UW) AWS	4415	72.58	38.46	3205	1987–96	107	Shuman et al. (2001)
Humboldt Gletscher	5	78.53	56.83	1995	1995–2003	91	Steffen et al. (1996)
Crawford Point (CP1)	2	69.88	46.97	2022	1995–2003	90	Steffen et al. (1996)
Swiss Camp	1	69.57	49.30	1149	1996–2004	89	Steffen et al. (1996)
Tunu-N	7	78.02	33.99	2020	1996–2003	87	Steffen et al. (1996)
DYE-2	8	66.48	46.28	2165	1996–2003	84	Steffen et al. (1996)
JAR1	9	69.50	49.68	962	1996–2003	81	Steffen et al. (1996)
Saddle	10	66.00	44.50	2559	1997–2003	80	Steffen et al. (1996)
Summit	6	72.58	38.50	3208	1996–2004	78	Steffen et al. (1996)
NASA-E	12	75.00	30.00	2631	1997–2003	72	Steffen et al. (1996)
NASA-SE	15	66.48	42.50	2579	1998–2003	68	Steffen et al. (1996)
NASA-U	3	73.83	49.50	2368	1995–2003	67	Steffen et al. (1996)
North Greenland Ice Sheet Project (NGRIP)	14	75.10	42.33	2950	1997–2003	62	Steffen et al. (1996)
South Dome	11	63.15	44.82	2922	1997–2003	61	Steffen et al. (1996)
JAR2	17	69.42	50.06	568	1999–2003	55	Steffen et al. (1996)
Camp Century	19	77.18	61.15	1885	1960–65	49	Ohmura (1987)
Site 2	7	77.00	56.08	2128	1953–57	47	Ohmura (1987)
Greenland Ice Training Site (GITS)	4	77.14	61.10	1887	1995–2003	44	Steffen et al. (1996)
JAR3	19	69.40	50.31	323	2000–03	43	Steffen et al. (1996)
CP2	13	69.91	46.85	1990	1997–2003	42	Steffen et al. (1996)
Station Centrale	5	70.92	40.63	2993	1949–51	24	Ohmura (1987)
Kangerdlugssuaq Accumulation Region (KAR)	16	69.70	33.00	2400	1992–2003	24	Steffen et al. (1996)
Northice	6	78.07	38.48	2343	1952–54	20	Ohmura (1987)
Jarl-Joset/Dumont	17	71.47	33.35	2867	1956–60	20	Ohmura (1987)
Tuto East	20	76.38	67.92	801	1961–63	19	Ohmura (1987)
Eismitte	1	70.90	40.70	3030	1930–31	12	Ohmura (1987)
Weststation Wegener	2	71.18	51.12	954	1930–31	12	Ohmura (1987)
Ice Cap Station Watkins	3	67.05	41.82	2440	1930–31	7	Ohmura (1987)
Kulusuk (KULU)	18	65.76	39.60	878	1999–2000	5	Steffen et al. (1996)
North Ice Cap Station II	10	76.92	66.97	650	1955–56	4	Ohmura (1987)
North Ice Cap Station III	11	76.93	66.98	700	1955–56	4	Ohmura (1987)
Hiran 29	15	68.07	42.33	2593	1956	4	Ohmura (1987)
Hiran 30	16	69.55	43.17	2558	1956	4	Ohmura (1987)
Hiran 26	12	68.25	36.50	2925	1956	3	Ohmura (1987)
Hiran 27	13	69.38	35.92	2755	1956	3	Ohmura (1987)
Hiran 28	14	70.62	36.17	3139	1956	3	Ohmura (1987)
Mint Julep	8	66.28	47.77	1829	1953	2	Ohmura (1987)
Sierra	9	77.23	62.33	1719	1953	2	Ohmura (1987)
Expedition Glaciologique Internationational au Groenland (EGIG) Camp IV	18	69.67	49.63	1004	1959	2	Ohmura (1987)
Camp Watkins	4	74.67	47.50	2659	1933	1	Ohmura (1987)

c. Polar MM5 regional climate model output

The fifth-generation Pennsylvania State University (PSU)–National Center for Atmospheric Research (NCAR) Mesoscale Model (MM5) has been modified for use in polar regions (Bromwich et al. 2001; Cassano et al. 2001). In the present 24-km horizontal grid resolution model configuration, Polar MM5 is reinitialized once per month and updated at the lateral boundaries using 6-hourly 2.5° horizontal resolution ERA-40 1958–2002 reanalyses and 12-hourly operational analyses for 2002–05. Tests we made indicate that the data frequency inconsistency between ERA-40 and ECMWF operational analyses does not produce problems for this study. The 12-hourly updates are adequate, as are the 6-hourly updates, in resolving synoptic-scale motions at the lateral boundaries, which usually change steadily. Further, we have found no significant difference between ERA-40 and ECMWF operational analyses from comparison studies. We use 3-hourly model output to produce monthly averages of air temperature calculated for a fixed height of 2 m above the surface. The present model configuration differs from that used in Box et al. (2004, 2006), as summarized by Table 3. The changed boundary layer and longwave schemes, the enhanced vertical resolution, the improved horizontal pressure gradient

TABLE 3. The comparisons between current 1958–2007 Polar MM5 version and that in Box et al. (2004, 2006).

Configuration/model	Previous model MM5 version 3.4	Present model MM5 version 3.7.3
Model restart	24-hourly model restarts	Monthly continuous simulations
Lateral boundary treatment	Linear interpolation between 12-h values	6 h
Output frequency	6 h	3 h
Initialization	ECMWF operational analysis	1957–2002 ERA-40 data and post-2002 ECMWF operational analysis data
Boundary layer scheme	Medium-Range Forecast (MRF) PBL	National Center for Environmental Prediction North American Model (formerly ETA Model)
Vertical resolution	28-level	35-level
Land surface classification	—	8-km GIMMS data (Tucker et al. 2005)
Horizontal pressure gradient	—	Higher-order calculation
Longwave scheme	CCM2	RRTM

calculation, and the land surface classification were implemented to improve the accuracy of the simulation. The consequences of running the simulations continuously for a month at a time are discussed below.

3. Methods

a. *Polar MM5 temperature errors and error minimization*

Before reconstruction techniques are applied, the 1958–2007 Polar MM5 temperature output errors are evaluated. Systematic error is modeled spatially and temporally such that it may be compensated. Residual error, that is, after the systematic pattern is subtracted, is used to gauge absolute uncertainty. We investigate the following sources of error: 1) the annual cycle of Polar MM5 minus monthly inland ice station records, 2) elevation-varying difference between simulated and in situ–observed temperature, 3) consistency of errors in time, and 4) spatial patterns of bias. Polar MM5 uses reanalysis data only for lateral boundary forcing. The reanalysis uses neither inland ice nor coastal station near-surface air temperature data, so the two are independent. Comparisons between simulated near-surface air temperature and station data are also made from before the 1958–2007 reconstruction training period. We assumed that there are no systematic biases in the in situ temperature observations. Consistency is tested by comparing biases from the first and second halves of the 1958–2007 reconstruction training period in addition to the 20-yr periods spanning 1840–2007. Spatial interpolation of regional bias patterns is made using kriging. Error analysis details are provided in the following subsections.

1) ANNUAL CYCLE OF TEMPERATURE ERROR

Over the annual cycle, a warm bias is evident at most sites and peaks in May, with minimum (or cold) biases in the period of October–February (Fig. 2). We believe that the source of the thermal bias is error in cloud amount/thickness that peaks in late spring when the Arctic is relatively cloud free (Serreze et al. 1998). A positive bias in Polar MM5–simulated downward longwave irradiance is evident in comparison with surface observations from Swiss Camp and Summit (not shown). The monthly Polar MM5 integration resulted in an overly developed cloud amount, in particular over the interior high elevations of the ice sheet where cloud radiative effect is minimal (Box 1997). An inland warm bias has been identified in ERA-40 data (Hanna et al. 2005). The inherent ERA-40 inland warm bias is derived at least partly from ~40 W m^{-2} positive bias in downward longwave radiation from the Rapid Radiative Transfer Model (RRTM) scheme used here in contrast to the NCAR Community Climate Model version 2 (NCAR CCM2) scheme, used previously in Polar MM5 (Hines and Bromwich 2008).

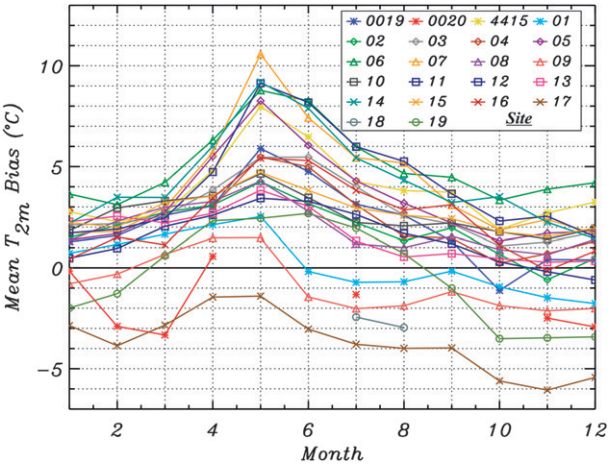

FIG. 2. Annual cycle of monthly multiyear average surface air temperature biases for selected ice stations during the 1958–2007 period. The site ID number from Table 2 is listed beside the symbol used.

2) TERRAIN-RELATED TEMPERATURE BIAS

Consistent with the coastal land station pattern, inland ice sites near the coast, having elevations less than about 1300 m, exhibit a cold bias (Fig. 3). The low-elevation/coastal cold bias becomes a warm bias above about 1100 m. Sites 17 (JAR2), 9 (JAR1), and 1 (Swiss Camp) are situated along an elevation transect near 69.5°N latitude and exhibit a distinct increase in cold bias as elevation decreases toward the ice margin. A cold bias is evident over land stations (not shown). Terrain-related absolute temperature bias is a typical regional climate model problem (e.g., Box and Rinke 2003; Box et al. 2004, 2006; Hanna et al. 2005) and stems partly from the need to smooth steep terrain to avoid atmospheric dynamical noise and violation of mass continuity. Furthermore, terrain smoothing occurs anyway in high-relief terrain by averaging high-resolution terrain data to a relatively coarse mesoscale model grid.

Polar MM5 has been configured to perform more skillfully in short-term forecast mode (e.g., Bromwich et al. 2001; Cassano et al. 2001). However, in the present case, faced with a computationally expensive 50-yr integration, a more efficient monthly integration was adopted at the apparent cost of reduced absolute accuracy. Fortunately, the bias patterns are largely systematic, and thus reasonably accurate interannual variability is maintained, and through calibration procedures absolute error can be minimized.

Previous studies employed slope lapse rates in temperature derived from in situ data (Steffen and Box 2001) to compensate for terrain-induced temperature bias. We instead use spatial interpolation of the monthly bias pattern to account for elevation-related error in addition to the apparent bias in terms of other factors such as regional climate, latitude, distance to the coast, slope aspect, etc. With this regional bias character in mind, note that the site 11 [South Dome Automatic Weather Station (AWS)] bias (Fig. 3) reflects the model trending to a coastal cold bias at the south of Greenland.

3) KRIGING OF SPATIAL BIAS PATTERNS

Kriging is an interpolation procedure that generates an estimated spatial surface from a scattered set of spatially distributed data points, using the covariance structure of the data to estimate interpolated values. Kriging interpolation procedures are applied to simulate regional bias patterns over the ice sheet for each month. The fits to spatial bias patterns are sensitive to the choices of the kriging parameters. For example, increasing the range value, that is, where the semivariogram sill is reached, increases the amount of spatial smoothing and can mask mesoscale features if the chosen value is too large. Decreasing the range retains increasingly local patterns, but can create unrealistic spatial patterns, especially where the local data coverage is sparse or clustered. After careful experimentation, a spherical model with a nugget of 0 K^2, a range of 22.5 grid lengths (540 km), and a sill value ranging from 0.1 to 5 K^2, depending on the monthly covariance, was then chosen for this interpolation procedure. Spatial bias patterns evolve consistently from month to month, allowing constant seasonal bias models to be chosen (Fig. 4) and to be constructed by averaging monthly bias models. The kriged pattern indicates a warm bias growing inland and a cold bias over the margins, in particular, over the extreme south and north ice sheet. Kriging also reproduces the maximum warm bias during spring and summer. The monthly kriged bias patterns are subtracted from Polar MM5 grids to simultaneously compensate for varying elevation and seasonal bias.

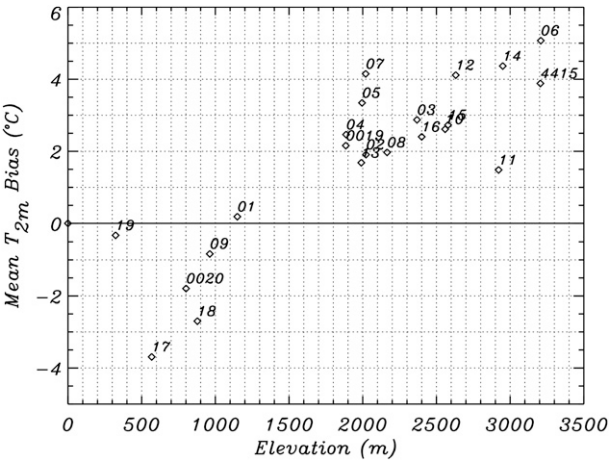

FIG. 3. Annual mean bias elevation distribution for over ice stations. The site ID number is placed at the upper right of the associated value.

b. Verification of error minimization

After the seasonal surface air temperature bias compensation is made, we remeasure error statistics to validate the error minimization and to quantify uncertainty. Apart from the relatively small residual February and March warm biases (up to 2°C) and an April cold bias (Fig. 5), which probably result from kriging imperfectly representing the spatial patterns of bias, we assume the residual error to be random anyway. Root mean squared error (RMSE) and bias values by season and elevation are tabulated in Table 4. Mean biases are half or less than half that of RMSE. RMSE remains within the range of 1.4°–1.8°C for sites below 1500-m elevation and 1.5°–2.0°C above 1500 m. Residual errors are smallest during spring and summer.

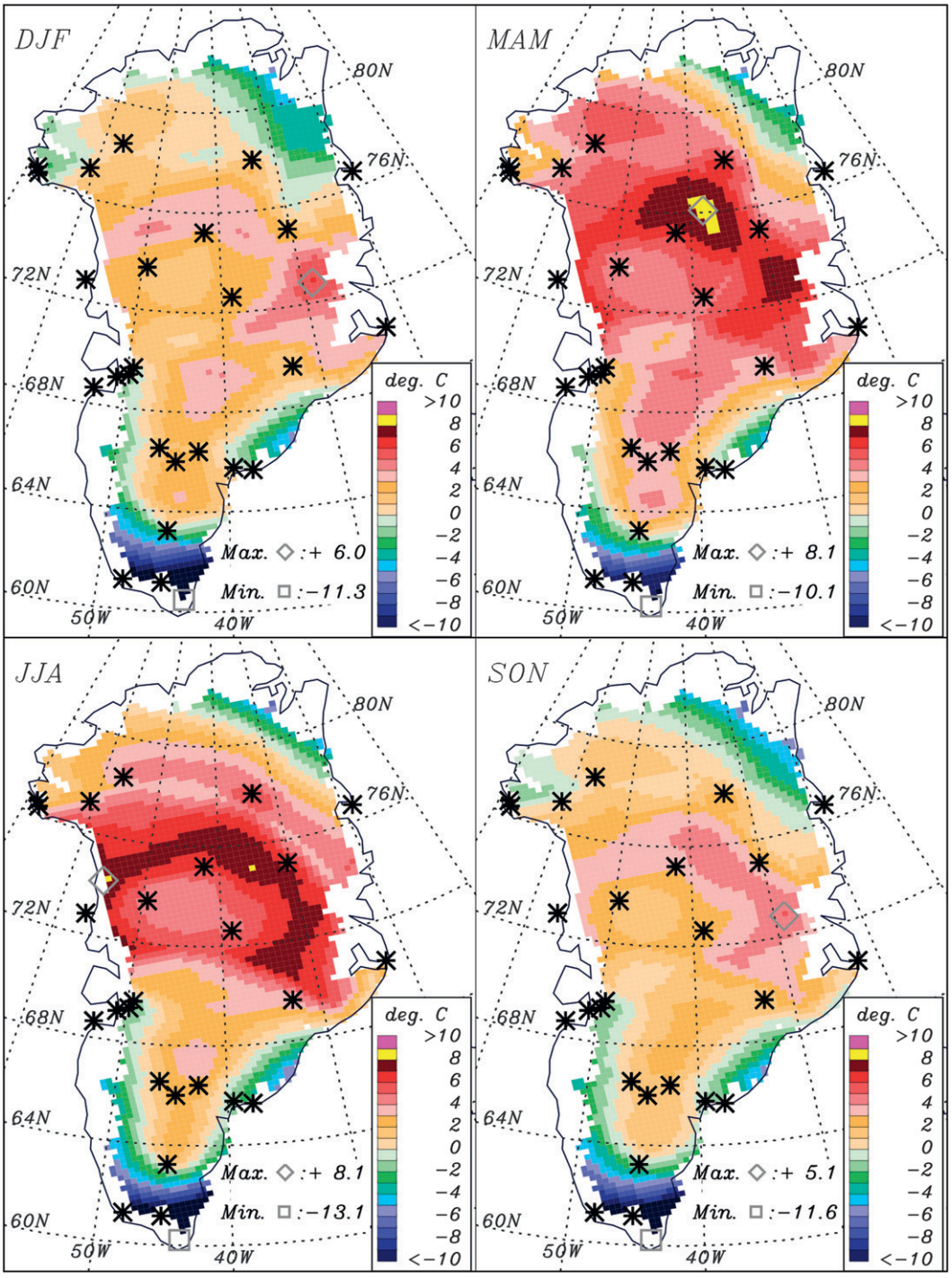

FIG. 4. Seasonal kriged bias pattern over ice grids (stars denote the stations used in kriging interpolation procedure).

c. *Interregression reconstruction*

Our reconstruction employs least squares fit parameters that describe a relationship between two time series, that is, the Polar MM5 output on a gridcell basis and from in situ point observations. The strength of long-term in situ observations is their relatively long temporal coverage, which is continuous for up to 168 yr at Ilulissat (1840–2007); there are five records that are longer than 100 yr (Table 1). Temperature records from

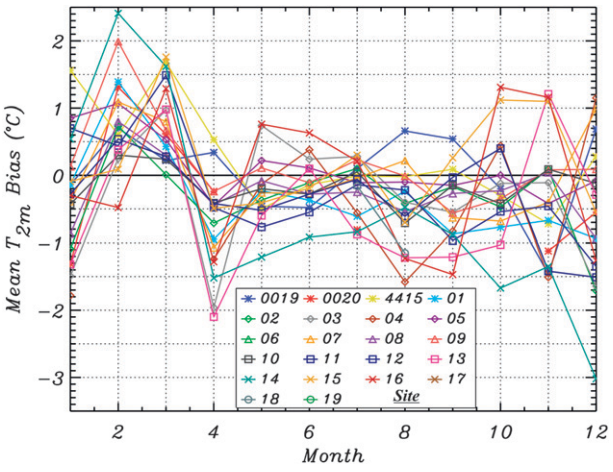

FIG. 5. Annual cycle of monthly multiyear average surface air temperature residual biases for the same ice stations as in Fig. 2 for the 1958–2007 period. The ice station number is included.

points in space provide incomplete/scant spatial coverage. Conversely, the Polar MM5 temperature series provide continuous spatial coverage, yet span a relatively short duration, that is, 50 yr. The data are combined in this reconstruction methodology to maximize their respective strengths with the longer-duration in situ records set as the explanatory variable. The dependent variable is chosen to be the bias-compensated Polar MM5 temperatures at 2937 inland ice grid points. The regression between both time series is evaluated in all possible combinations, that is, between all Polar MM5 grid points and all meteorological station records. A 24-km grid of 55 × 101 containing the correlation values for each meteorological training site is stored for later use in reconstruction. The sites' Pearson's correlation coefficients (R) are ranked on a gridcell basis in order to best explain the Polar MM5 temporal variability. The highest-ranked site for which data are available in a given month and year are used in the reconstruction. The reconstruction thus maximizes reproductive skill, yet remains flexible to account for variable data availability at monthly time intervals. Table 1 lists the driving data availability. In the earliest period of reconstruction, that is, pre-1873, the whole-Greenland reconstruction depends on variability information from just three sites, that is, Ilulissat, Nuuk, and Qaqortoq. In the post-1873 period, three more sites become available for the reconstruction. After 1965, 11 sites drive the reconstruction. We present reconstructions from 1840 onward, despite some data being available as early as 1784. The fraction of the total Greenland area that each coastal record represents is discussed later.

d. Stationarity of reconstructed temperature errors

Different subintervals of the 50-yr overlap are employed to evaluate the effect of the sample period (and size) on the reconstructed values given that a key assumption of the reconstruction is that the relationship between the simulated and observed interannual air temperature variability as represented by empirical functions is stationary in time. The presatellite (1948–78) and satellite (1979–2005) eras are considered first, because we suspected the presatellite accuracy for ERA-40 to be less, given that satellite remote sensing offers more spatially dense horizontal and vertical temperature and water vapor profiles and sea surface temperatures used by ERA-40. The average bias for the selected stations decreases by 56%, that is, from 0.23° to 0.13°C from the presatellite era to the satellite era (Fig. 6c). We might tentatively conclude that the satellite-era analysis data produce a more accurate reconstruction. However, the RMSE does not decrease and other data aspects, such as changing in situ air temperature sensor types and changing spatial sample distribution, are likely additional causes of time differences in the apparent model error.

To search for multidecadal shifts in uncertainty, 20-yr interval comparisons are made between the time series of reconstructed temperature at eight stations with 50+ yr records. To maximize time span, the 20-yr periods extend backward in time from the latest year (2007). Figures 6b,d illustrate how reconstructed temperature uncertainty does not vary systematically over the 1.5-century reconstruction period. Detection of temperature trends seems limited to those greater in magnitude than the 0.4°C RMSE.

e. Time series analysis

Periods of apparent temperature trends are compared in terms of magnitude and duration. Trend periods are

TABLE 4. Postcalibration error statistics by season and elevation range (°C).

Season	December–February (DJF)		March–May (MAM)		June–August (JJA)		September–November (SON)	
Statistics	Bias	RMSE	Bias	RMSE	Bias	RMSE	Bias	RMSE
<1500 m	0.6	1.5	−0.3	1.4	−0.5	0.9	−0.6	1.8
>1500 m	0.3	2.0	−0.4	1.8	−0.3	1.5	−0.4	1.7

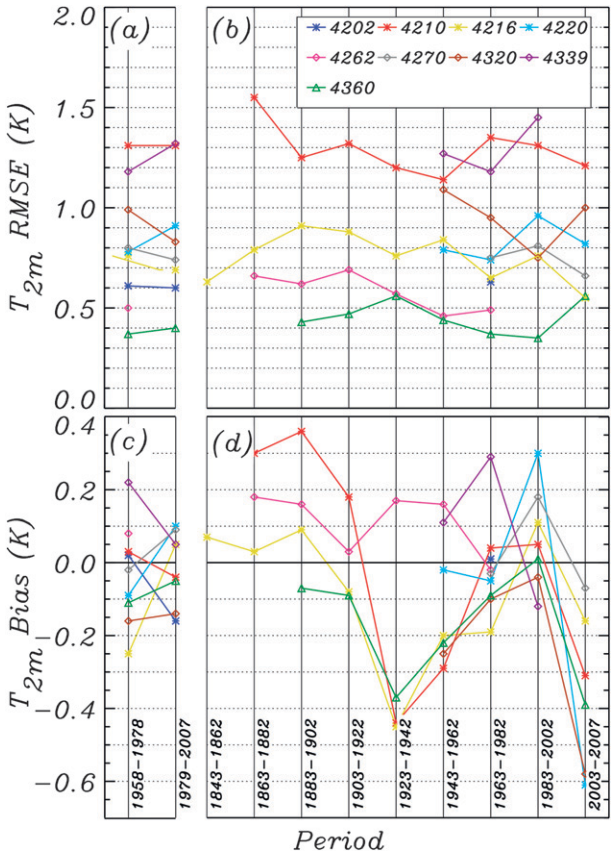

FIG. 6. The 2-m annual RMSE and bias for different time intervals for selected stations.

chosen carefully to avoid times that are affected by volcanism. In some trend periods, volcanism cannot be avoided. Whether the trend is for a period that is apparently strongly influenced by volcanism is indicated in the tabulated results. Temperature anomalies are calculated relative to the 1951–80 base period. A 30-yr period is considered a ''climate normal'' sufficient to establish a long-term mean. Further, this period is chosen because it has relatively small trends. Note that selection of the base period influences the magnitude of neither the anomalies nor the trends.

To evaluate interdecadal fluctuations, a 6°C standard deviation 31-yr Gaussian-weighted running mean smoothing filter is used. Within 15 yr of the time series beginning or end, the tail on the Gaussian sample (i.e., ''boxcar'') is truncated by one in each year toward the end until the sample size is 15. We later refer to this filter as ''low pass,'' that is, allowing low-frequency variability to pass through the filter.

A trailing Gaussian running mean was chosen first but was abandoned because it shifted signals (such as caused by volcanic episodes) to earlier years and produced a noisier time series. Despite the fact that the two-tailed Gaussian running mean includes future data points unphysically, no spurious patterns were apparent when comparing the two- and one-tailed running mean results.

f. Regional analysis

Results, such as trend magnitude and interannual anomalies are tabulated on a basin scale. We use ice sheet drainage basin areas based on Zwally and Giovinetto (2001; Fig. 1) to assist in identifying glaciologically significant regions of temperature variability.

4. Results and discussion

a. Regional temperature correlation

Geographically coherent gridcell maximum regression skill patterns are evident. The correlation between the time series of temperature at a meteorological station and the Polar MM5 grid over the 1958–2007 period includes patterns of distance decay of correlation, maritime versus land correlation differences, orography, and storm tracks. The longest correlation length scales are found in winter. Short correlation length scales in summer are indicative of the more relaxed macroscale pressure fields (Serreze et al. 1993) and the damping effects of melting on sensible heat variability (e.g., Steffen 1995). At Ilulissat, for example, a high correlation is evident across the western slope of Greenland (Fig. 7), more so in autumn and winter than in other seasons. Coherent site maximum correlation patterns are also consistent with climatological regions separated by the ice sheet topographic divide. Along the eastern slope of the ice sheet, the Illulisat correlation is minimal.

Elsewhere, at Tasiilaq, east Greenland is favored by the reconstruction methodology, exhibiting spatial and seasonal correlation patterns (Fig. 8) consistent with for example, Ilulissat (Fig. 7). Correlations between Polar MM5 and the station record are higher over land than sea, suggesting a decoupling of land and sea climate variability. Tasiilaq correlates better with oceanic regions in summer than inland regions. Again, the latent heat sink of surface melt is a major candidate factor, although it would not explain the absence of strong correlation over the high inland ice sheet where there is essentially no melting.

Figure 9 illustrates which of the century-plus training site records most skillfully represent the Polar MM5 seasonal temperature variability. The same patterns are evident when shorter-duration sites are added. The downstream advection of airmass characteristics is apparent in the spatial correlation patterns, given that the prevailing wind direction aloft is southwesterly. Thus,

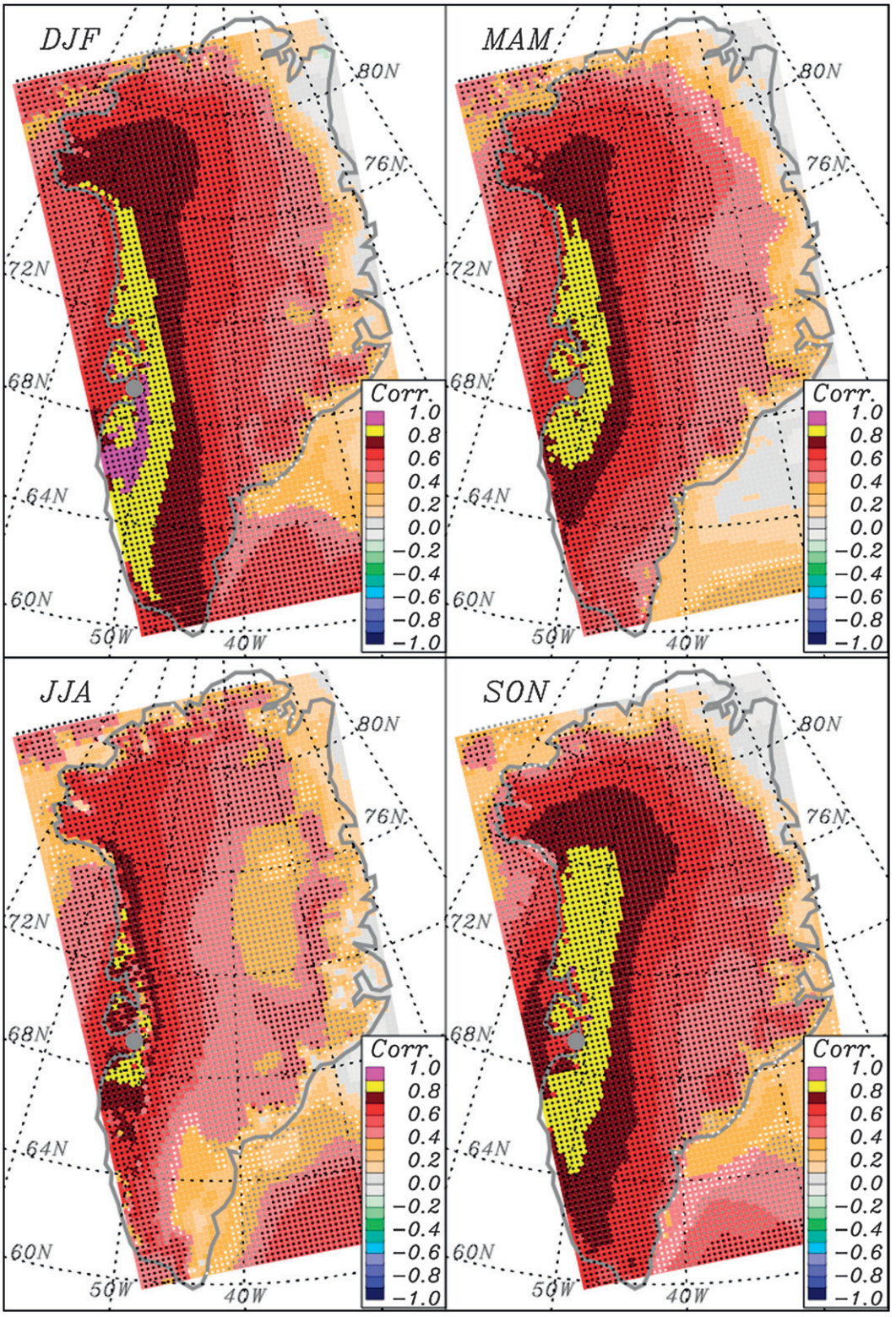

FIG. 7. Seasonal correlation patterns for 1958–2007 of the Ilulissat meteorological station recorded surface air temperature observations vs Polar MM5–modeled 2-m air temperature. Dotted grid cells indicate confidence of statistical significance, white dots indicate ≥90% confidence. Gray dots indicate confidence ≥95%, and black dots indicate confidence ≥99%.

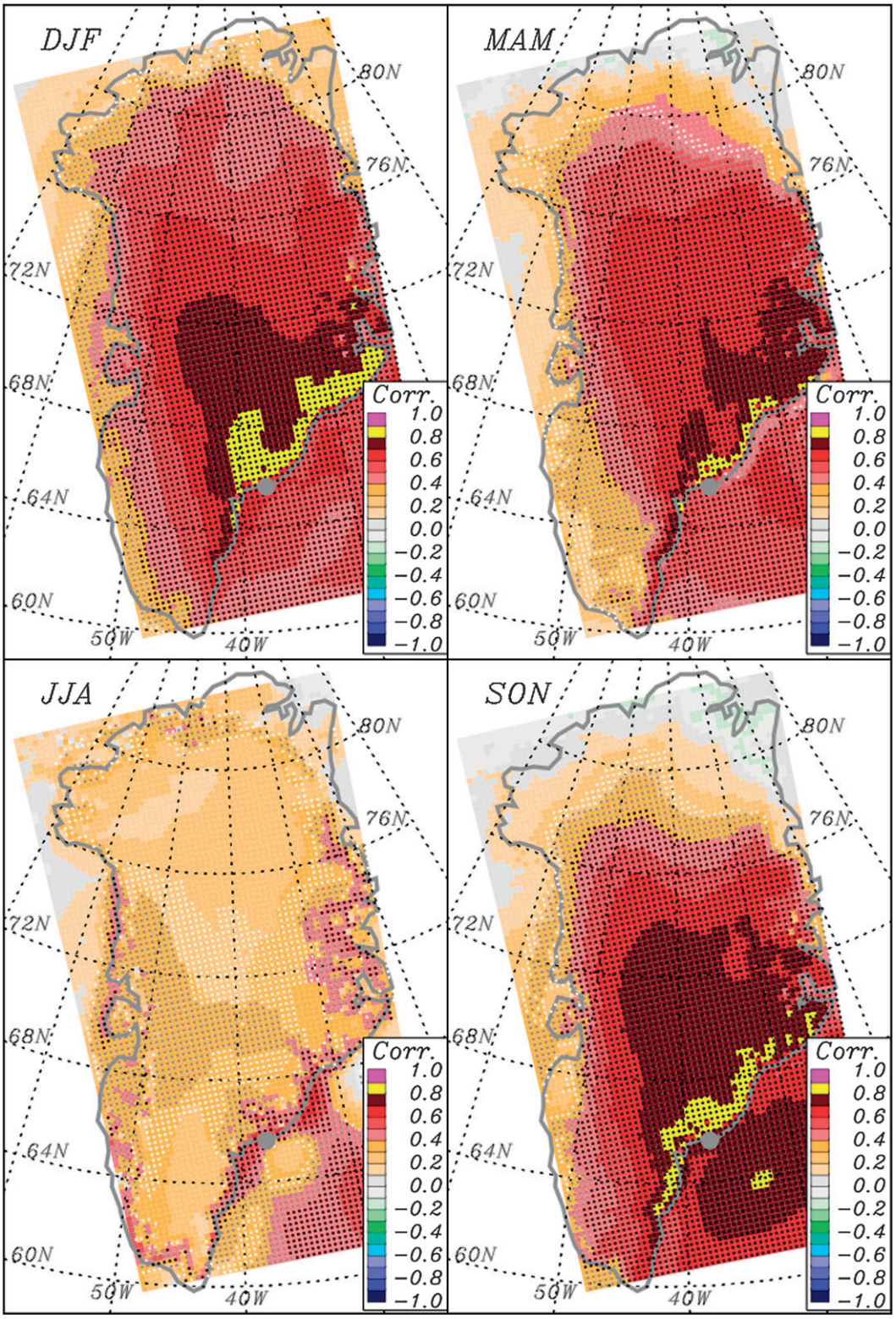

FIG. 8. As in Fig. 7, but for the Tasiilaq meteorological station.

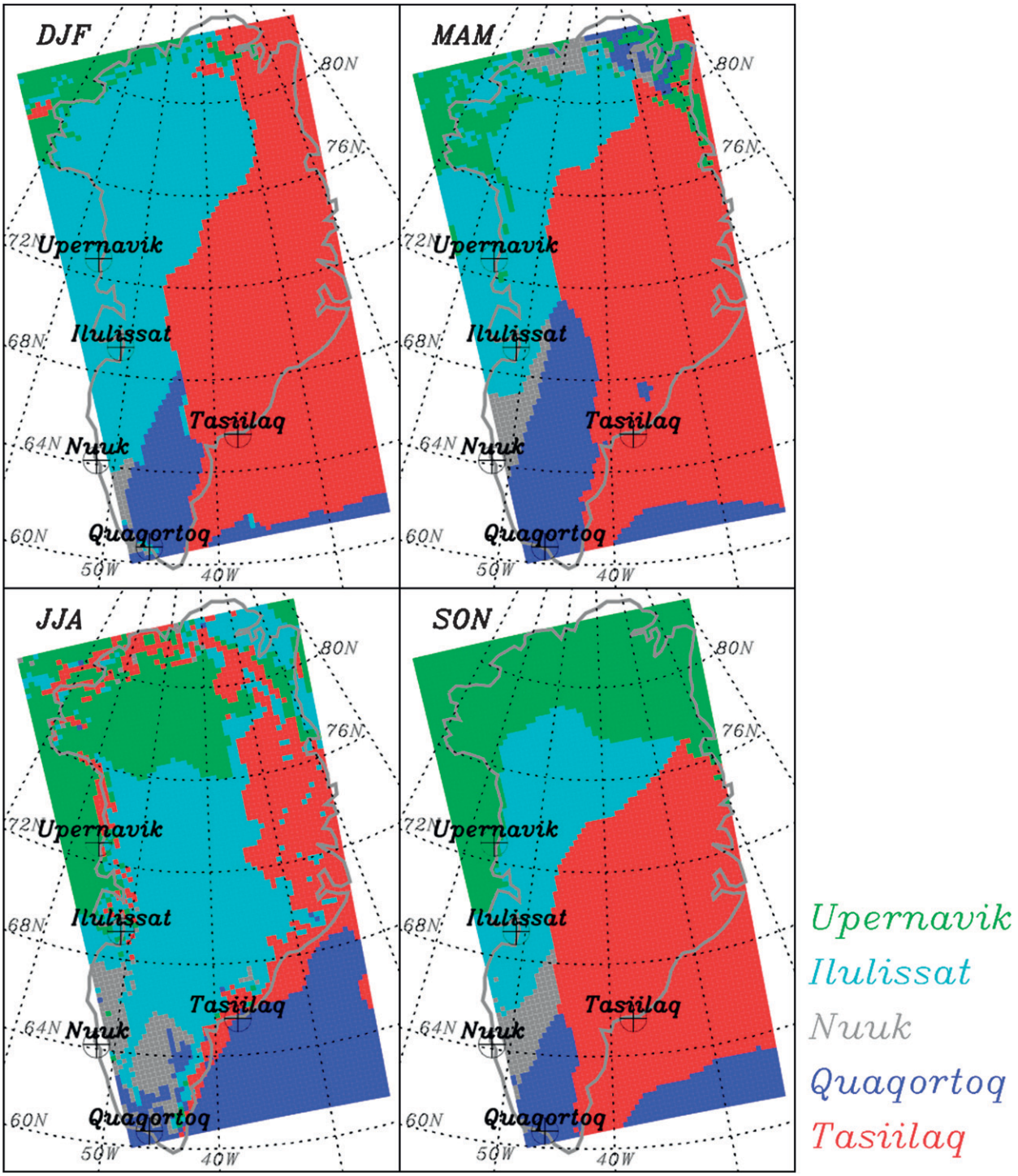

FIG. 9. Seasonal spatial patterns of highest-ranking reproduction sites for sites with records longer than 100 yr.

western sites better explain the inland ice gridcell temperature variability in time (see also Figs. 7 and 8). It is beneficial to this reconstruction methodology that the most skillful sites include those (Ilulissat and Tasiilaq) for which relatively long uninterrupted temperature series are available. Nuuk best represents the southwestern land area but is minimally skillful over the inland ice. We believe that Nuuk's lower correlation reflects the more maritime climate resulting from its island locality and the relatively wide and high-elevation landmass

TABLE 5. The 2-m Anomaly ranges for each basin over 1840–2007 (°C).

Basin	South	Northwest	Southwest	Southeast	East	Northeast	North	Whole
Anomaly range	1.6	2.3	2.1	1.7	1.7	1.4	1.9	1.8

isolating it from the inland ice influence. In the majority of seasons, Pittufik better explains the inland ice temperature variability above Upernavik, which, like Nuuk, better represents local maritime climate than terrestrial or inland ice locations. Also noteworthy is that Danmarkshavn outperforms other sites in representing the northeast ice sheet (not shown).

b. *Annual temperature variability*

Basin-scale ranges of annual temperature (Table 5) indicate an overall ice sheet annual average surface air temperature range of 1.8°C, providing context that a, for example, 2°C annual warming (see Gregory et al. 2004) would be extreme in the historical context. Regionally, the largest temperature ranges (range greater than 2°C) are found along the western ice sheet. Minimal ranges are evident for the northeast where the role of sea ice is thought to be an important modulator of surface air temperatures (Cappelen et al. 2001). We speculate that south Greenland temperature variability is relatively small because of a less strong winter influence, bearing in mind that largest interannual variability is evident in winter (Box 2002; Fig. 10).

c. *Seasonal temperature variability*

Smoothed seasonal and annual temperature time series indicate substantial interdecadal positive and negative trends (Fig. 10). Annual means are dominated by winter variability, which is 5 times greater than the summer range over the 1840–2007 period. Again, stronger winter variability is linked with a more vigorous atmospheric circulation (Serreze et al. 1993), that is, with the more frequent and rapid passage of cold and warm air masses. The stronger winter equator-to-pole temperature difference is the root cause of the stronger winter circulation. Summer temperature variability is lower because of the less vigorous atmospheric circulation (smaller equator-to-pole temperature differential), and the fact that once surface melting begins, sensible heat is sunk into melting and damping surface air temperature variability (Steffen 1995). Summer temperatures thus have a ceiling of variability. Nevertheless, nonsummer (nonmelt season) temperature variability can still affect summer melt rates via modulating snowpack and ice "cold content," that is, colder snow requires more energy input before the melting point is reached (e.g., Pfeffer et al. 1991).

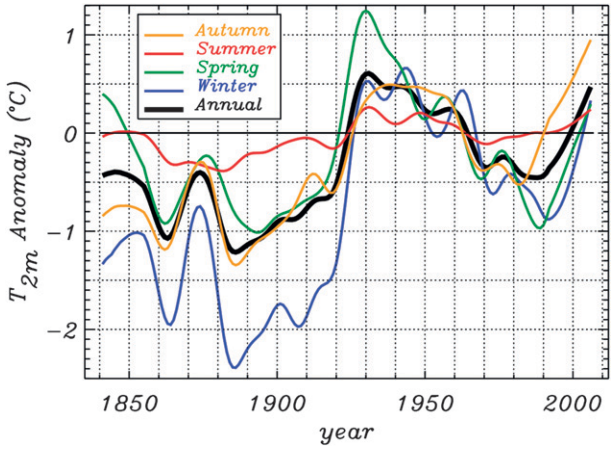

FIG. 10. Gaussian filtering of Greenland ice sheet annual 2-m temperature anomalies relative to the 1951–80 base period.

d. *Air temperature trends*

A number of apparently coherent multiannual trend periods are evident in the temperature time series for the ice sheet (Fig. 10). We chose periods in ways to avoid the effect of short-lived volcanic cooling episodes (Table 6). Warming trend periods are evident: 1885–1919, 1862–73, 1919–32, and 1994–2007. Two interdecadal cooling periods are 1932–46 and 1955–82. The 1955–82 cooling phase was most significant during autumn in east and southern Greenland. The 1932–46 cooling phase was relatively weak and not statistically significant. The 1862–73 warming trend is strong, and strongest in winter, especially for western regions (the southwest and northwest), and to a lesser extent in spring.

While trends above 1500-m elevation tend to be somewhat larger in magnitude than those below 1500 m (not shown), we tabulate values for the whole ice sheet and on a basin scale (Table 6).

e. *Interdecadal temperature variability influenced by volcanism*

Cooling during 1–3 yr volcanic episodes produces negative anomalies that in most cases exceed three standard deviations from the 1951–80 mean (Fig. 11). The cool anomalies exceed five standard deviations in the case of the Krakatau eruption and the apparent 1861–63 effect of the Makian Island, Halmahera, Indonesia eruption. A few smaller negative spikes do not appear to be synchronous with volcanic eruptions, for

TABLE 6. Whole ice sheet and basin-scale seasonal and annual temperature changes (°C per period). Italicized values indicate confidence of statistical significance ≥90% confidence. Bold values indicate confidence ≥95%. Underlined values indicate confidence ≥99%.

Period	Season/basin	Whole	North	Northeast	East	Southeast	Southwest	Northwest	South
1862–73 warming, active volcanism	DJF	***4.0***	***4.7***	***2.9***	***2.2***	*3.0*	***5.2***	***5.9***	*3.9*
	MAM	1.8	1.3	0.9	1.1	***2.0***	***2.9***	2.2	***2.6***
	JJA	0.3	0.5	0.3	0.2	0.2	0.3	0.6	0.3
	SON	*2.2*	*2.5*	*1.7*	1.3	*1.8*	*2.8*	3.4	1.7
	Annual	***2.1***	***2.3***	***1.5***	*1.2*	***1.8***	***2.8***	***3.0***	***2.1***
1919–32 warming, no major volcanism	DJF	***3.8***	***4.6***	***2.6***	***3.5***	***3.5***	***4.1***	***5.0***	2.8
	MAM	***3.6***	***3.3***	***3.1***	***4.0***	***3.4***	***4.1***	***3.9***	***3.6***
	JJA	***1.1***	***1.1***	***0.8***	***1.0***	***1.1***	***1.2***	***1.1***	***1.2***
	SON	1.0	1.0	0.7	1.3	1.3	1.1	0.6	*2.0*
	Annual	***2.4***	***2.5***	***1.8***	***2.5***	***2.3***	***2.6***	***2.7***	***2.4***
1932–46 cooling	DJF	0.4	0.4	0.2	0.0	0.4	0.9	0.2	1.9
	MAM	−0.9	−1.6	−0.6	0.0	−0.3	−1.2	*−1.9*	−0.9
	JJA	*−0.4*	−0.3	−0.2	−0.4	*−0.4*	−0.5	*−0.4*	−0.5
	SON	0.1	−0.5	0.2	1.0	0.6	0.1	−0.7	−0.3
	Annual	−0.2	−0.5	−0.1	0.2	0.1	−0.2	−0.7	0.1
1955–82 cooling	DJF	−0.5	−0.1	*−1.2*	−0.7	−0.2	0.0	−0.2	0.3
	MAM	−0.8	0.4	−0.6	*−1.3*	***−1.3***	*−1.2*	−0.2	***−1.6***
	JJA	−0.1	−0.1	0.0	−0.1	−0.2	−0.3	0.0	*-0.4*
	SON	*−1.1*	−0.3	−0.6	***−1.7***	***−1.7***	***−1.6***	−0.8	***−1.5***
	Annual	*−0.6*	0.0	***−0.6***	*−1.0*	***−0.9***	*−0.8*	−0.3	*−0.8*
1994–2007 warming, no major volcanism	DJF	***3.8***	***2.8***	***2.8***	***3.0***	***3.9***	***5.2***	***4.4***	***5.2***
	MAM	1.5	***1.7***	0.9	1.5	*1.4*	***1.8***	***1.9***	*1.8*
	JJA	***0.8***	***0.9***	***0.6***	***0.7***	***0.8***	***0.9***	***0.8***	***0.7***
	SON	1.1	1.3	1.2	0.9	1.1	1.1	1.3	0.9
	Annual	***1.8***	1.7	***1.4***	***1.5***	***1.8***	***2.3***	***2.1***	***2.2***

example, 1938 and 1949. Further, the 1963 Mount Agung eruption, which Hanna et al. (2005) noted had a damping effect on ice sheet melt rates, is apparent in the reconstructed winter means only (Fig. 10).

Post-volcanic surface air temperature changes over the Northern Hemisphere are mostly the result of the altered atmospheric dynamics. Shortwave radiation absorption by volcanic aerosols heat the tropical lower stratosphere, increasing the strength of the polar vortex, in turn leading to a shift in the planetary wave pattern in the stratosphere (Hines 1974; Robock 2000). Regionally, our reconstruction reproduces volcanic cooling concentrated in western Greenland, and is consistent with the findings from instrumental records (Robock and Mao 1995; Box 2002). Seasonally, we find that the lower-tropospheric volcanic cooling is strongest during the dynamically active season of winter. Seasonal air temperature anomalies for the August 1883 Krakatau volcanic episode are illustrated (see Fig. 12). Simulations in Rozanov et al. (2002, Fig. 14d) lend confidence to the idea that amplified west Greenland cooling is real, and that the cause is related to the vertical energy balance between the stratosphere and troposphere. The topographic and thermal influence of the ice sheet are important in anchoring planetary wave circulation (Bromwich et al. 1996; Kristjansson and McInnes 1999) and, we speculate, contributing to the observed and simulated west Greenland concentration of volcanic cooling.

f. Comparison of 1920s and 1990s warming periods

The two strongest warming periods since 1840 are identified as 1919–32 and 1994–2007, each lasting 14 yr

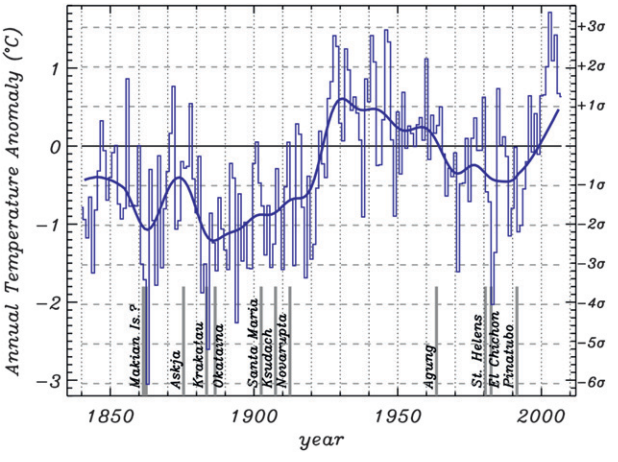

FIG. 11. Greenland ice sheet land station record annual temperature anomalies with respect to the 1951–80 base period. Multiples of standard deviations for the 1951–80 period are included. Major volcanic eruptions are indicated.

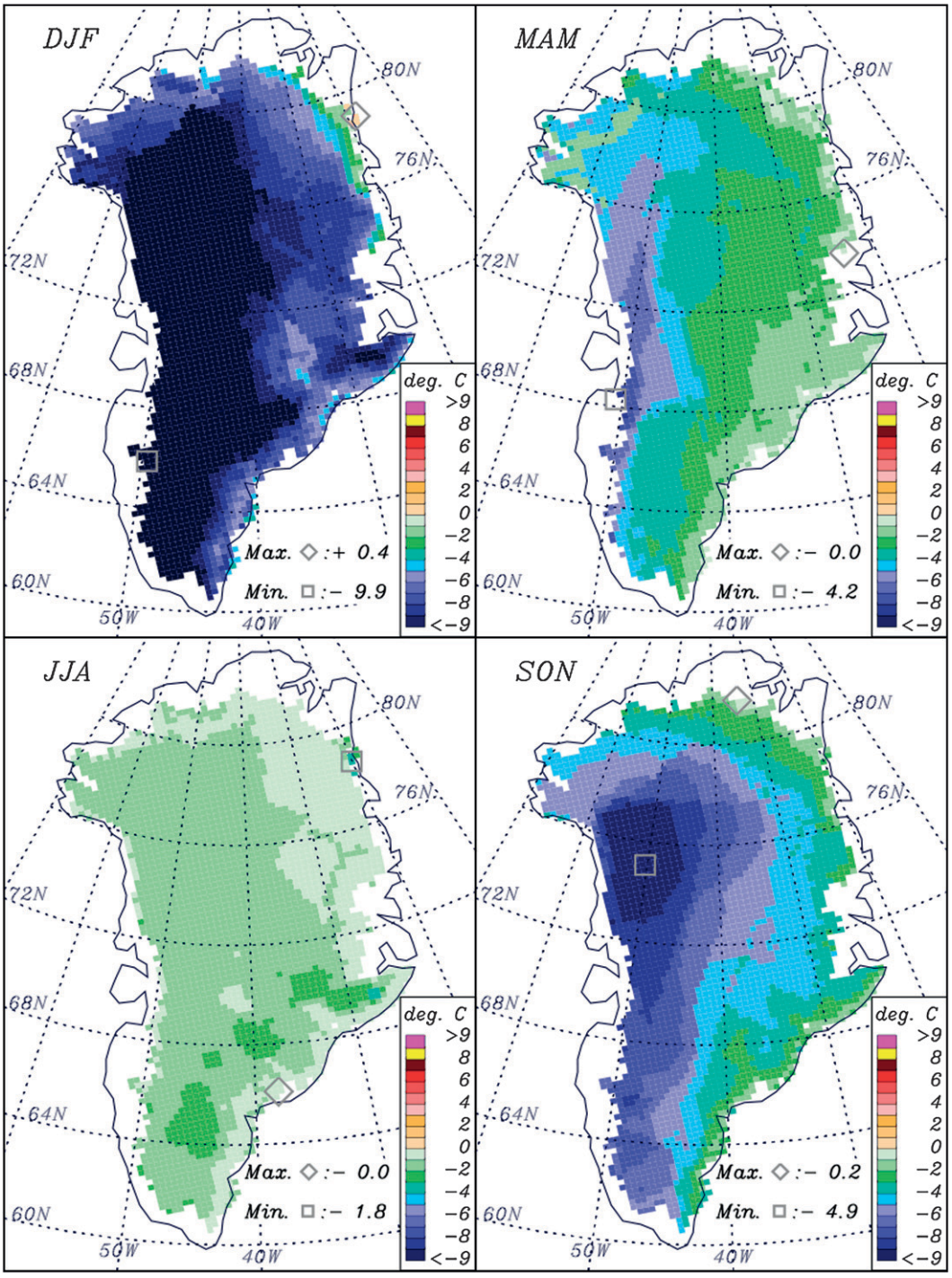

FIG. 12. Seasonal 2-m air temperature anomalies for 1884 with respect to the 1840–58 base period.

for simplicity of comparison. Annual temperature anomalies in both cases are more than two standard deviations (2σ) above the 1951–80 base (Fig. 11).

The 1919–32 warming was larger in magnitude overall than the 1994–2007 warming; it was 0.6°C greater annually for the whole ice sheet and greater regionally, in particular, by 0.6°C in winter and 2.0°C in spring for the northwest part of the ice sheet (Fig. 13, Table 6). The 1994–2007 warming was larger, however, over the southern part of the ice sheet in winter, that is, by 2.4°C (see Table 6).

Differences between the 1919–32 and 1994–2007 warming periods include that the former is marked by

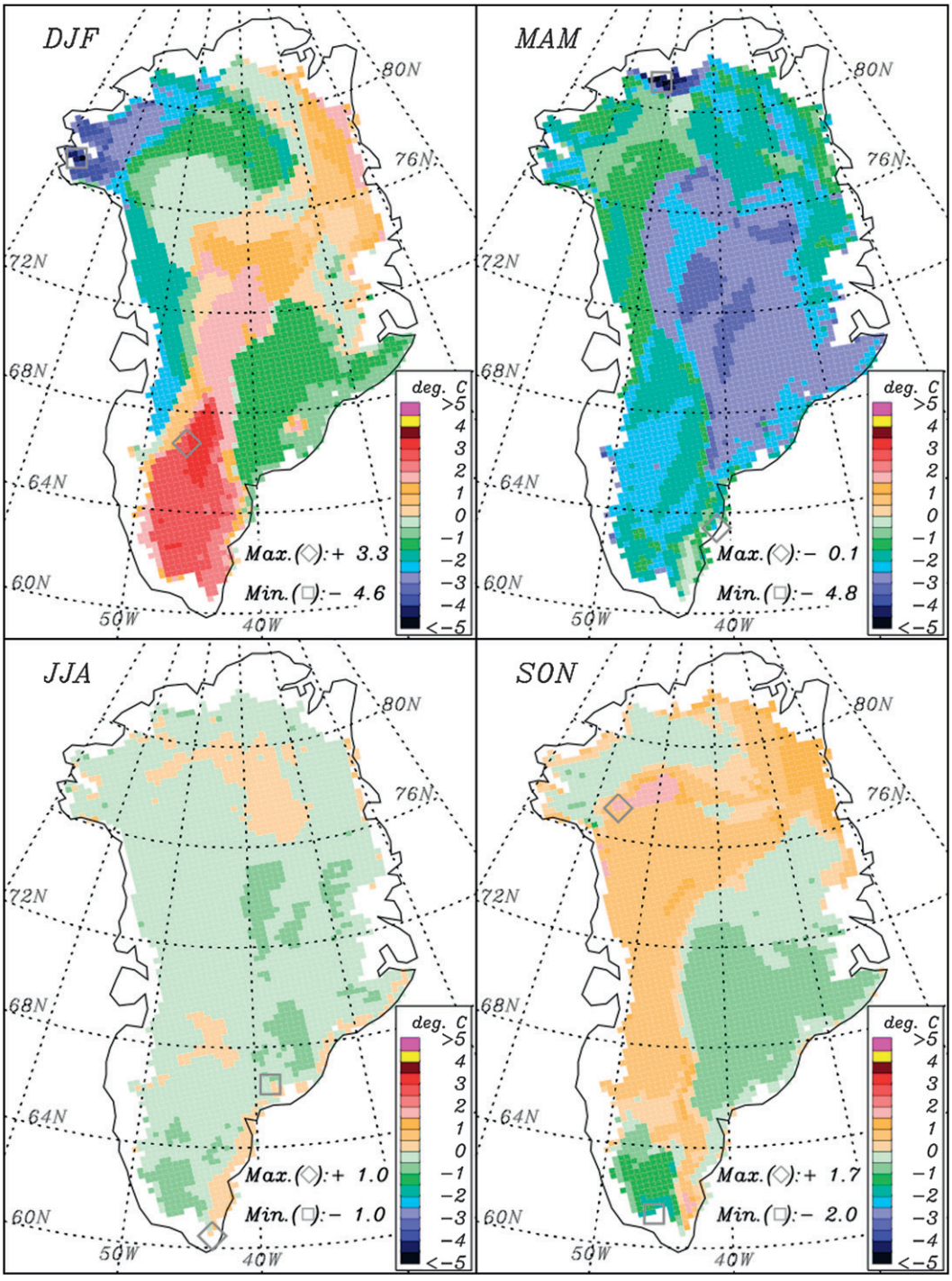

FIG. 13. Difference between warming trends, that is, the 1994–2007 temperature change (from linear regression of all years) minus the 1919–32 change.

spring warming, leading other seasons in time by a few years (Fig. 10). The 1919–32 winter warming is larger in overall magnitude, with spring reaching the most positive anomaly of all seasons. During the 1994–2007 warming, autumn leads other seasons by several years. Furthermore, for the period of 1994–2007, the temperature anomaly for autumn is more positive than the other seasons. Winter is the final season to catch up to the annual average for both the 1919–32 and 1994–2007 warming period (Fig. 10).

TABLE 7. Seasonal and basin-scale surface air temperature change ratio (1919–32)/(1994–2007). The region with greatest absolute departure is bold and underlined.

Season/basin	Whole	North	Northeast	East	Southeast	Southwest	Northwest	South
DJF	1.00	1.64	0.93	1.17	0.90	0.79	1.14	**0.54**
MAM	2.40	1.94	**3.44**	2.67	2.43	2.28	2.05	2.00
JJA	1.38	1.22	1.33	1.43	1.38	1.33	1.38	**1.71**
SON	0.91	0.77	0.58	1.44	1.18	1.00	0.46	**2.22**
Annual	1.32	**1.49**	1.31	1.61	1.29	1.17	1.26	1.12

Both the 1919–32 and the post-1993 warming coincide with an absence of volcanic cooling (see Fig. 11). Warming rates between the 1994–2007 and 1919–32 periods are compared using the ratio of the change both seasonally and on a basin scale in Table 7. The greatest difference between the two warming periods is the factor of 2 or larger spring warming in 1919–32 versus 1994–2007 (Fig. 12, Table 7). In autumn, the extreme south warmed more (factor of 2.2) in 1919–32 versus 1994–2007. In contrast, the extreme southern part of the ice sheet winter warming rate was nearly 2 times greater during 1994–2007 than 1919–32. If glacier response is greater in summer than winter, one might expect a greater retreat of Greenland glaciers in 1919–32 than 1994–2007. While no satellite observations are available from the 1920s, what observations exist from oblique aerial photos, maps, and paintings do indicate a 1920s–1940s Greenland glacier retreat (Box and Herrington 2007).

g. *Comparison between Greenland and the Northern Hemisphere*

Global and NH warming 1975–2007 has been attributed to the dominance of increased greenhouse and solar forcing over various cooling factors (Solomon et al. 2007). High-latitude warming is simulated by global climate models to be amplified by the ice albedo feedback (Budyko 1969; Solomon et al. 2007). NH cooling 1940–70 has been attributed primarily to the dominance of sulfate aerosol cooling sourced from increased coal-fired power plants largely in the Western Hemisphere (Wild et al. 2005, 2007), and partly to decreasing solar activity during that period (Solomon et al. 2007). Subsequent warming is attributed primarily to increasing greenhouse gasses while coal-fired power plant SO_2 emissions were reduced. Whether sulfate aerosols directly or indirectly cooled west Greenland, that is, far away from industrial sources, is something we address in our interpretation.

During the 1881–2006 period, Greenland ice sheet temperature anomalies are in phase with NH anomalies the majority of the time ($R = 0.658$; see Fig. 14). The time correlation of the two series would be higher were it not for apparent decadal-scale lags between the two. Noteworthy phase exceptions are that Greenland temperatures were still cooling during the 1970s and 1980s, years after NH temperatures began warming, highlighting the relatively strong influence of volcanic cooling on Greenland versus the NH. Given the phase agreement the majority of the time, we further explore if recent warming is of a similar character to the 1919–32 warming in an effort to understand what may be in store for Greenland in the coming decade. The Greenland mid-twentieth-century smoothed anomalies peaked in 1931 at 0.61°C above the 1951–80 base period, while those of the NH peaked in 1941. The Greenland peak was 4.5 times greater than the NH peak. We use this ratio as an estimate of proportionality between the two time series. Another proportionality estimate is based on the regression between the NH and Greenland, which suggests that Greenland has, on average, a factor of 1.6 greater magnitude of variability.

$$T_{\text{Anom, Greenland Ice Sheet}} = -1.557_{T\text{anom, NH}} + 0.658.$$

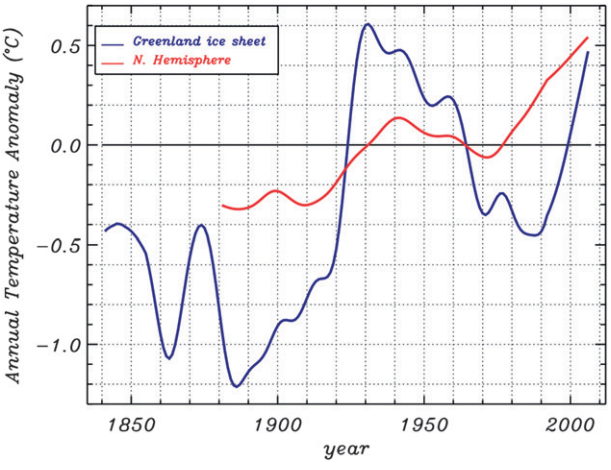

FIG. 14. Time series of low-pass-filtered Greenland inland ice and Northern Hemisphere near-surface air temperature anomalies with respect to the 1951–80 base period.

The mid-twentieth-century Greenland temperature anomalies surpassed those of the NH average in 1923. The crossover occurred as if Greenland temperatures are closely in phase with the NH. In contrast, the 1994–2007 Greenland warming has not surpassed the NH anomaly. If Greenland warming was in phase and proportion with the NH pattern, using the mid-twentieth-century ratio between Greenland and NH peak temperatures, we calculate that an anomaly of 2.1°C above the 1951–80 mean, or an additional 1.6°C Greenland warming above the 2006 anomaly, would be required. Alternatively, according to the regression, the 2006 Greenland air temperature anomaly should be 1.5°C, or 1.0°C above the actual 2006 ice sheet air temperature anomaly.

Given that recent climate warming has already pushed the Greenland ice sheet mass budget into a deficit, from increasing surface meltwater runoff (Box et al. 2006; Hanna et al. 2008) and accelerated tidewater glacier discharge (see Zwally et al. 2002; Luthcke et al. 2006; Rignot and Kanagaratnam 2006; Howat et al. 2008; Joughin et al. 2008; Rignot et al. 2008), additional warming would most certainly increase the total ice sheet mass deficit. Assuming 1.5°C warming in Greenland, that is, for Greenland climate to be in proportion with the NH trend, we expect a net decrease in the surface mass input by 30 Gt, owing to the dominance of increased ablation over increased snow accumulation (Box et al. 2004; Fettweis et al. 2008; Hanna et al. 2008). A ~15-Gt increase in solid precipitation is expected for each 1°C warming (Box et al. 2004). An additional 45-Gt meltwater runoff may seem small compared to the major loss term of iceberg discharge of ~386 Gt (Rignot and Kanagaratnam 2006), but the interplay of melt and glacier discharge (Zwally et al. 2002; Joughin et al. 2008; Rignot et al. 2008) need be recognized. The surface mass budget has recently approached negative values in abnormally warm years (see, e.g., Box et al. 2006; Fettweis et al. 2008), for example, with relatively little west Greenland precipitation (i.e., during 2003). Meanwhile, increased outlet glacier discharge is adding more than any isolated mass budget term to the increasing total mass deficit (e.g., Luthcke et al. 2006; Velicogna and Wahr 2006; Rignot et al. 2008). How far the ice sheet mass budget is perturbed beyond its threshold of viability (Gregory et al. 2004) will continue to be a subject of critical interest.

5. Conclusions

Long-term Greenland ice sheet 2-m near-surface air temperature reconstruction is enabled by combining available station records and independent regional climate model output in ways that leverage their respective strengths. Greenland instrumental surface air temperature records span 168 yr continuously, that is, 1840–2007. Polar MM5 simulations spanning 1958–2007 are used to represent spatial distributions in surface air temperature. The correlation between stations and model grids exhibits distinct distance-decay patterns, with the lowest correlation length scales and inland ice penetration during summer when melting creates a ceiling of variability and atmospheric circulation is least vigorous. Western stations are presumably more representative of the central inland ice than eastern sites given the prevailing southwesterly flow over most of the southern ice sheet. Fortunately, the higher performance sites for the reconstruction also had the longest records.

Observational records, independent in space and time of the Polar MM5 output, facilitate genuine uncertainty assessment and spatial interpolation to compensate systematic biases. Stationarity tests indicate that the effect of data inhomogeneity is negligible, with no coherent variation in RMS uncertainty in 20-yr periods spanning 1860–2007. Residual temperature reconstruction biases evident from comparisons with independent data suggest that the absolute annual whole ice sheet bias is less than ±0.4°C. Local 20-yr RMSE values are less than 1.6°C.

Over the 1840–2007 time span, two multidecadal low-temperature periods (1861–1919 and 1963–84) in Greenland coincide with periods of multiple major volcanic eruptions. Greenland is most sensitive to volcanic (sulfate) cooling during the dynamically active winter season and along the western ice sheet margin, that is, when the equator-to-pole temperature differential is strongest and owing to the ice sheet topographic and baroclinic effect of planetary wave anchoring, respectively. Considering also that Northern Hemispheric cooling in 1940–70 is attributable to the ''global dimming'' effect of increasing sulfate aerosols, the sulfate cooling effect is, again, felt more strongly in Greenland, and indirectly via altered atmospheric dynamics not via local radiation budget modification. The topographic and thermal influence of the ice sheet are important in anchoring planetary wave circulation (Bromwich et al. 1996; Kristjansson and McInnes 1999) and, we speculate, contributing to the observed and simulated (Rozanov et al. 2002) west Greenland concentration of volcanic cooling.

Consistent with previous studies, the 1920s annual warming trend is found to be larger in magnitude, that is, by a factor of 1.33, as compared to 1994–2007 warming. In contrast, the 1994–2007 winter warming was 1.7 times greater in magnitude over southern Greenland in than 1919–32.

Greenland ice sheet annual temperature anomalies are more than a factor of 2 greater than Northern Hemisphere anomalies or 1.6 times greater according to statistical regression. In the early twentieth-century warming, Greenland anomalies surpassed the Northern Hemisphere anomalies in 1923, with close phase agreement between the two time series. In contrast, recent (1994–2007) regional warming around Greenland has not surpassed the hemispheric anomaly. Using the empirical relationships between Greenland and the Northern Hemisphere surface air temperature data, we calculate that if Greenland was to become in phase with the hemispheric pattern, as it did after 1923, an additional 1.0°–1.6°C warming would occur. In light of this prediction and global climate model forecasts for continued high-latitude warming, the ice sheet mass budget deficit is likely to continue to grow in the coming decades. With the exception of major volcanic eruptions, cooling caused by a negative phase of the Atlantic Multidecadal Oscillation and/or NAO (Hanna and Cappelen 2003) and strong decreases in solar output are the only potential regional climate trends (Keenlyside et al. 2008) we are aware of to moderate Greenland deglaciation.

Climate warming has pushed the Greenland ice sheet beyond its threshold of viability in recent years (Rignot et al. 2008). The ice sheet seems poised not to grow without substantial regional and global climate cooling. It therefore seems much more likely that not that Greenland is and will be for the foreseeable future be a deglaciating Pleistocene Ice Age relic.

Acknowledgments. This work was supported by Cryospheric Sciences Program of NASA's Earth Science Enterprise Grant NNG04GH70G. We thank Edward Hanna and two anonymous reviewers. Discussion with Eugene Rozanov of Observatory and World Radiation Center (PMOD/WRC), Switzerland were enlightening.

REFERENCES

Bindoff, N. L., and Coauthors, 2007: Observations: Oceanic climate change and sea level. *Climate Change 2007: The Physical Science Basis,* S. Solomon et al., Eds., Cambridge University Press, 387–429.

Box, J. E., 1997: Polar day effective cloud opacity in the Arctic from measured and modeled solar radiation fluxes. M.S. thesis, Department of Geography, University of Colorado, 111 pp.

——, 2002: Survey of Greenland instrumental temperature records: 1873-2001. *Int. J. Climatol.,* **22,** 1829–1847.

——, and A. Rinke, 2003: Evaluation of Greenland ice sheet surface climate in the HIRHAM regional climate model. *J. Climate,* **16,** 1302–1319.

——, and A. E. Cohen, 2006: Upper-air temperatures around Greenland: 1964–2005. *Geophys. Res. Lett.,* **33,** L12706, doi:10.1029/2006GL025723.

——, and A. Herrington, 2007: Was there a 1930's meltdown of Greenland glaciers? *Eos, Trans. Amer. Geophys. Union,* **88** (Fall Meeting Suppl.), Abstract C11A-0077.

——, D. H. Bromwich, and L.-S. Bai, 2004: Greenland ice sheet surface mass balance 1991–2000: Application of Polar MM5 mesoscale model and in situ data. *J. Geophys. Res.,* **109,** D16105, doi:10.1029/2003JD004451.

——, and Coauthors, 2006: Greenland ice sheet surface mass balance variability (1988–2004) from calibrated Polar MM5 output. *J. Climate,* **19,** 2783–2800.

Bromwich, D. H., Y. Du, and K. M. Hines, 1996: Wintertime surface winds over the Greenland ice sheet. *Mon. Wea. Rev.,* **124,** 1941–1947.

——, J. Cassano, T. Klein, G. Heinemann, K. Hines, K. Steffen, and J. E. Box, 2001: Mesoscale modeling of katabatic winds over Greenland with the Polar MM5. *Mon. Wea. Rev.,* **129,** 2290–2309.

Budyko, M. I., 1969: The effects of solar radiation on the climate of the earth. *Tellus,* **21,** 611–619.

Cappelen, J., B. V. Jørgensen, E. V. Laursen, L. S. Stannius, and R. S. Thomsen, 2001: The observed climate of Greenland, 1958–99, with climatological standard normals, 1961–90. Danish Meteorological Institute Tech. Rep. 00-18, 152 pp.

——, E. V. Laursen, P. V. Jørgensen, and C. Kern-Hansen, 2006: DMI monthly climate data collection 1768-2005, Denmark, The Faroe Islands and Greenland. Danish Meteorological Institute Tech. Rep. 06-09, 53 pp.

Cassano, J., J. E. Box, D. H. Bromwich, L. Li, and K. Steffen, 2001: Verification of Polar MM5 simulations of Greenland's atmospheric circulation. *J. Geophys. Res.,* **106,** 33 867–33 890.

Chylek, P., M. K. Dubey, and G. Lesins, 2006: Greenland warming of 1920–1930 and 1995–2005. *Geophys. Res. Lett.,* **33,** L11707, doi:10.1029/2006GL026510.

Crowley, T. J., 2000: Causes of climate change over the past 1000 years. *Science,* **289,** 270–277.

Csatho, B., T. Schenk, C. J. Van der Veen, and W. B. Krabill, 2008: Intermittent thinning of Jakobshavn Isbrae, West Greenland since the Little Ice Age. *J. Glaciol.,* **54,** 131–144.

Fettweis, X., E. Hanna, H. Gallée, P. Huybrechts, and M. Erpicum, 2008: Estimation of the Greenland ice sheet surface mass balance during 20th and 21st centuries. *Cryosphere,* **2,** 225–254.

Fichefet, T., C. Poncin, H. Goosse, P. Huybrechts, I. Janssens, and H. Le Treut, 2003: Implications of changes in freshwater flux from the Greenland ice sheet for the climate of the 21st century. *Geophys. Res. Lett.,* **30,** 1911, doi:10.1029/2003GL017826.

Gregory, J. M., P. Huybrechts, and S. C. B. Raper, 2004: Threatened loss of the Greenland Ice Sheet. *Nature,* **428,** 616, doi:10.1038/428616a.

Hanna, E., and J. Cappelen, 2003: Recent cooling in coastal southern Greenland and relation with the North Atlantic Oscillation. *Geophys. Res. Lett.,* **30,** 1132, doi:10.1029/2002GL015797.

——, P. Huybrechts, I. Janssens, J. Cappelen, K. Steffen, and A. Stephens, 2005: Runoff and mass balance of the Greenland Ice Sheet: 1958–2003. *J. Geophys. Res.,* **110,** D13108, doi:10.1029/2004JD005641.

——, and Coauthors, 2008: Increased runoff from melt from the Greenland Ice Sheet: A response to global warming. *J. Climate,* **21,** 331–341.

Hansen, J., R. Ruedy, J. Glascoe, and M. Sato, 1999: GISS analysis of surface temperature change. *J. Geophys. Res.,* **104,** 30 997–31 022.

——, ——, M. Sato, M. Imhoff, W. Lawrence, D. Easterling, T. Peterson, and T. Karl, 2001: A closer look at United States and global surface temperature change. *J. Geophys. Res.,* **106,** 23 947–23 963.

Hines, C. O., 1974: A possible mechanism for the production of sun–weather correlations. *J. Atmos. Sci.,* **31,** 589–591.

Hines, K. M., and D. H. Bromwich, 2008: Development and testing of Polar WRF. Part I: Greenland ice sheet meteorology. *Mon. Wea. Rev.,* **136,** 1971–1989.

Holland, D. M., R. H. Thomas, B. deYoung, M. H. Ribergaard, and B. Lyberth, 2008: Acceleration of Jakobshavn Isbrae triggered by warm subsurface ocean waters. *Nature Geosci.,* **1,** 659–664, doi:10.1038/ngeo316.

Howat, I. M., I. Joughin, M. Fahnestock, B. E. Smith, and T. Scambos, 2008: Synchronous retreat and acceleration of southeast Greenland outlet glaciers 2000-2006; Ice dynamics and coupling to climate. *J. Glaciol.,* **54,** 646–660.

Jones, P. D., M. New, D. E. Parker, S. Martin, and I. G. Rigor, 1999: Surface air temperature and its changes over the past 150 years. *Rev. Geophys.,* **37,** 173–199.

Joughin, I., W. Abdalati, and M. Fahnestock, 2004: Large fluctuations in speed on Greenland's Jakobshavn Isbræ glacier. *Nature,* **432,** 608–610.

——, S. B. Das, M. A. King, B. E. Smith, I. M. Howat, and T. Moon, 2008: Seasonal speedup along the western flank of the Greenland ice sheet. *Science,* **320,** 781–783.

Kahl, J. D., M. C. Serreze, R. S. Stone, S. Shiotani, M. Kisley, and R. C. Schnell, 1993: Tropospheric temperature trends in the Arctic: 1958–1986. *J. Geophys. Res.,* **98** (D7), 12 825–12 838.

Kaufman, D. S., and Coauthors, 2004: Holocene thermal maximum in the western Arctic (0-180°W). *Quat. Sci. Rev.,* **23,** 529–560, doi:10.1016/j.quascirev.2003.09.007.

Keenlyside, N. S., M. Latif, J. Jungclaus, L. Kornblueh, and E. Roeckner, 2008: Advancing decadal-scale climate prediction in the North Atlantic sector. *Nature,* **453,** 84–88.

Kristjansson, J. E., and H. McInnes, 1999: The impact of Greenland on cyclone evolution in the North Atlantic. *Quart. J. Roy. Meteor. Soc.,* **125,** 2819–2834.

Lemke, P., and Coauthors, 2007: Observations: Changes in snow, ice and frozen ground. *Climate Change 2007: The Physical Science Basis*, S. Solomon et al., Eds., Cambridge University Press, 339–378.

Luthcke, S. B., and Coauthors, 2006: Recent Greenland ice mass loss by drainage system from satellite gravity observations. *Science,* **314,** 1286–1289.

Moon, T., and I. Joughin, 2008: Changes in ice front position on Greenland's outlet glaciers from 1992 to 2007. *J. Geophys. Res.,* **113,** F02022, doi:10.1029/2007JF000927.

Oerlemans, J., and H. F. Vugts, 1993: A meteorological experiment in the melting zone of the Greenland ice sheet. *Bull. Amer. Meteor. Soc.,* **74,** 355–365.

Ohmura, A., 1987: New temperature distribution maps for Greenland. *Z. Gletscherkd. Glazialgeol.,* **23,** 1–45.

——, and Coauthors, 1991: Energy and mass balance during the melt season at the equilibrium line altitude, Paakitsoq, Greenland Ice Sheet. Department of Geography, Swiss Federal Institute of Technology Progress Rep. 1, 108 pp.

Peterson, T. C., and R. S. Vose, 1997: An overview of the Global Historical Climatology Network temperature database. *Bull. Amer. Meteor. Soc.,* **78,** 2837–2849.

Pfeffer, W. T., M. F. Meier, and T. H. Illangasekare, 1991: Retention of Greenland runoff by refreezing: Implications for projected future sea level change. *J. Geophys. Res.,* **96** (C12), 22 117–22 124.

Przybylak, R., 1997: Spatial and temporal changes in extreme air temperatures in the Arctic over the period 1951–1990. *Int. J. Climatol.,* **17,** 615–634.

Putnins, P., 1970: The climate of Greenland. *Climates of the Polar Regions*, S. Orvig, Ed., Vol. 14, *World Survey of Climatology*, Elsevier, 3–113.

Rahmstorf, S., and Coauthors, 2005: Thermohaline circulation hysteresis: A model intercomparison. *Geophys. Res. Lett.,* **32,** L23605, doi:10.1029/2005GL023655.

Rignot, E., and P. Kanagaratnam, 2006: Changes in the velocity structure of the Greenland ice sheet. *Science,* **311,** 986–990.

——, J. E. Box, E. Burgess, and E. Hanna, 2008: Mass balance of the Greenland ice sheet from 1958 to 2007. *Geophys. Res. Lett.,* **35,** L20502, doi:10.1029/2008GL035417.

Robock, A., 2000: Volcanic eruptions and climate. *Rev. Geophys.,* **38,** 191–219.

——, and J. Mao, 1995: The volcanic signal in surface temperature observations. *J. Climate,* **8,** 1086–1103.

Rozanov, E. V., M. E. Schlesinger, N. G. Andronova, F. Yang, S. L. Malyshev, V. A. Zubov, T. A. Egorova, and B. Li, 2002: Climate/chemistry effects of the Pinatubo volcanic eruption simulated by the UIUC stratosphere/troposphere GCM with interactive photochemistry. *J. Geophys. Res.,* **107,** 4594, doi:10.1029/2001JD000974.

Serreze, M. C., J. E. Box, R. G. Barry, and J. E. Walsh, 1993: Characteristics of Arctic synoptic activity, 1952-1989. *Meteor. Atmos. Phys.,* **51,** 147–164.

——, J. R. Key, J. E. Box, J. A. Maslanik, and K. Steffen, 1998: A new monthly climatology of global radiation for the Arctic and comparisons with NCEP–NCAR reanalysis and ISCCP-C2 Fields. *J. Climate,* **11,** 121–136.

Shuman, C., K. Steffen, J. E. Box, and C. R. Stearns, 2001: A dozen years of temperature observations at the summit: Central Greenland automatic weather stations 1987–99. *J. Appl. Meteor.,* **40,** 741–752.

Solomon, S., D. Qin, M. Manning, Z. Chen, M. Marquis, K. B. Averyt, M. Tignor, and H. L. Miller, 2007: *Climate Change 2007: The Physical Science Basis*. Cambridge University Press, 996 pp.

Steffen, K., 1995: Surface energy exchange at the equilibrium line on the Greenland ice sheet during onset of melt. *Ann. Glaciol.,* **21,** 13–18.

——, and J. E. Box, 2001: Surface climatology of the Greenland ice sheet: Greenland Climate Network 1995–1999. *J. Geophys. Res.,* **106** (D24), 33 951–33 964.

——, ——, and W. Abdalati, 1996: Greenland Climate Network: GC-Net. Special Report on Glaciers, Ice Sheets, and Volcanoes, Cold Regions Research and Engineering Laboratory Rep. 96-27, 98–103.

Tucker, C. J., E. Pinzon, M. E. Brown, D. A. Slayback, E. W. Pak, R. Mahoney, E. F. Vermote, and N. El Saleous, 2005: An extended AVHRR 8-km NDVI data set compatible with MODIS and SPOT vegetation NDVI data. *Int. J. Remote Sens.,* **26,** 4485–4498.

van de Wal, R. S. W., W. Boot, M. R. van den Broeke, C. J. P. P. Smeets, C. H. Reijmer, J. J. A. Donker, and J. Oerlemans, 2008: Large and rapid velocity changes in the ablation zone of the Greenland ice sheet. *Science,* **321,** 111–113.

Velicogna, I., and J. Wahr, 2006: Acceleration of Greenland ice mass loss in spring 2004. *Nature,* **443,** 329–331, doi:10.1038/nature05168.

Vinther, B. M., K. K. Andersen, P. D. Jones, K. R. Briffa, and J. Cappelen, 2006: Extending Greenland temperature records into the late eighteenth century. *J. Geophys. Res.,* **111,** D11105, doi:10.1029/2005JD006810.

Wild, M., and Coauthors, 2005: From dimming to brightening: Decadal changes in solar radiation at Earth's surface. *Science,* **308,** 847–850.

——, A. Ohmura, and K. Makowski, 2007: Impact of global dimming and brightening on global warming. *Geophys. Res. Lett.,* **34,** L04702, doi:10.1029/2006GL028031.

Zwally, H. J., and M. B. Giovinetto, 2001: Balance mass flux and ice velocity across the equilibrium line in drainage systems of Greenland. *J. Geophys. Res.,* **106** (D24), 33 717–33 728.

——, W. Abdalati, T. Herring, K. Larson, J. Saba, and K. Steffen, 2002: Surface melt-induced acceleration of Greenland ice sheet flow. *Science,* **297,** 218–222.